atmosphere

MDPI

Article

Evasion of Gaseous Elemental Mercury from Forest and Urban Soils Contaminated by Historical and Modern Ore Roasting Processes (Idrija, Slovenia)

Federico Floreani [1], Elena Pavoni [1], Mateja Gosar [2] and Stefano Covelli [1,*]

[1] Department of Mathematics and Geosciences, University of Trieste, Via Weiss 2, 34128 Trieste, Italy; federico.floreani@units.it (F.F.); epavoni@units.it (E.P.)
[2] Geological Survey of Slovenia, Dimičeva ulica 14, 1000 Ljubljana, Slovenia; mateja.gosar@geo-zs.si
* Correspondence: covelli@units.it; Tel.: +39-040-5582031

Abstract: Considerable amounts of gaseous elemental mercury (Hg^0) can be released into the atmosphere from Hg-enriched substrates, such as those from former mining areas, posing a potential environmental threat. In this work, Hg^0 fluxes at the soil–air interface under natural vegetation covers were measured in various locations within the Idrija Hg mining area (Slovenia) and its surroundings. Sites were selected in order to compare Hg^0 fluxes from both forest soils heavily impacted by historical ore roasting and urban soils characterised by a different degree of Hg enrichment due to the natural occurrence of Hg in rocks or recent mining and roasting processes. Replicate measurements at each site were conducted using a non-steady state flux chamber coupled with a real-time Hg^0 analyser (Lumex RA-915M). Moreover, topsoil samples (0–2 cm) were analysed for Hg total concentration and speciation. Cinnabar was the predominant Hg form in almost all the sites. Despite Hg^0 being undetectable in soils using thermo-desorption, substantial emissions were observed (70.7–701.8 ng m^{-2} h^{-1}). Urban soils in a naturally enriched area showed on average the highest Hg^0 fluxes, whereas relatively low emissions were found at the historical roasting site, which is currently forested, despite the significantly high total Hg content in soils (up to 219.0 and 10,400 mg kg^{-1}, respectively). Overall, our findings confirm that shading by trees or litter may effectively limit the amount of Hg^0 released into the atmosphere even from extremely enriched soils, thus acting as a natural mitigation.

Keywords: legacy soil contamination; Hg mining; gaseous Hg fluxes; flux chamber; ore roasting; Hg speciation

Citation: Floreani, F.; Pavoni, E.; Gosar, M.; Covelli, S. Evasion of Gaseous Elemental Mercury from Forest and Urban Soils Contaminated by Historical and Modern Ore Roasting Processes (Idrija, Slovenia). *Atmosphere* **2023**, *14*, 1036. https://doi.org/10.3390/atmos14061036

Academic Editors: Xinbin Feng, Jerry Lin, Xuewu Fu and Wei Zhu

Received: 10 May 2023
Revised: 12 June 2023
Accepted: 14 June 2023
Published: 16 June 2023

1. Introduction

Past mining and metallurgical activities have led to heavy and widespread mercury (Hg) contamination of all environmental media (soil, water, and air) in the surrounding areas [1–3]. The occurrence of Hg in the environment represents a serious concern due to its potential bioaccumulation via trophic webs and its negative effects on the health of both humans and ecosystems, particularly in its organic methylated form [4–6].

A peculiarity of this metal is the high volatility of its elemental form (Hg^0), which is easily released into the atmosphere from natural surfaces after the reduction in oxidised forms (Hg^{2+}) that are dominant in terrestrial and aquatic environments [7,8]. Due to its stability in the atmosphere, Hg^0 represents the most abundant form of Hg in this compartment (where it is usually abbreviated as GEM, Gaseous Elemental Mercury [9]) and can persist for a considerable period of time (0.6–2 years) before being removed via wet and dry depositions [10,11]. Consequently, Hg^0 can be subjected to long-range atmospheric transport even in remote ecosystems [12–14]. Moreover, deposed Hg can be re-emitted back into the atmosphere after its reduction to Hg^0, further increasing the spatial distribution of

Hg and making it a pollutant of global concern, as recognised by the Minamata Convention in 2013 [15,16].

A notable source of Hg^0 into the atmosphere is represented by emissions from the natural surfaces of substrates enriched in Hg due to natural geology or past mining and industrial activities [15,17], where Hg^0 fluxes can reach values of up to thousands of ng m^{-2} h^{-1} [18–21]. However, direct measurements of Hg^0 fluxes from these substrates are still scarce [22,23]. A more profound understanding of the processes that lead to the release of high amounts of Hg from these sites is of interest both on a local scale to prevent the occurrence of high atmospheric Hg concentrations and on a global scale to better understand the dispersion of this metal in the environment [18,24–26].

One of the most important drivers of Hg^0 emissions at contaminated sites is represented by total Hg concentrations in the substrate [15]. However, many other factors can influence the magnitude of Hg^0 fluxes at the soil–air interface, including the intensity of solar radiation [24], soil and air temperature [27,28], rainfall and soil moisture [29,30], and soil cover by vegetation [18]. The relative importance of all these factors in influencing Hg^0 fluxes is extremely site-specific [7].

Slovenia is known for its numerous mines and ore processing sites that were active in the second half of the 19th century and in the first quarter of the 20th century [31]. Later, most were closed and abandoned as the ore reserves were depleted. The oldest mining town is Idrija, where Hg ore was mined for 500 years until 1994 when the rotary furnace was in operation for the last time. During the long period of mining and ore processing, a large geochemical halo of Hg was created. Several research projects conducted over the last two decades confirmed the high levels of Hg in all environmental compartments. The soil is highly contaminated (exceeding 10 mg kg^{-1}) over an area of more than 20 km^2 [32,33] and detailed research on urban soil in Idrija showed that Hg concentrations were extremely high, ranging from about 10 to 1550 mg kg^{-1} [34,35].

The spread of Hg in the environment varies with time. Before mining activities started, the levels of Hg in the environment were only slightly heightened due to natural geogenic conditions. This occurred mostly in the area of natural outcrop of rocks containing native Hg and cinnabar (called "Pront" area) in the south-western part of the town of Idrija. However, the contribution of Hg-rich soil parent material to present-day Hg contamination is likely to be relatively limited, as this naturally enriched area is relatively small (approximately 4000 m^2) [32,36–38]. Conversely, the most important factors influencing Hg spreading in the environment are where and how the ore is processed. In the first decade of mining, ore was roasted at the site of an open pit, which is now located in the town center of Idrija, and the first roasting residue dumps with high Hg content were deposited on the banks of the Nikova and Idrijca Rivers. Because of the high demand for wood, part of the ore was transported to the surrounding forests from the early 16th century to the mid-17th century and roasted there. Initially, the ore was roasted in piles and later in earthen vessels. During both processes, about half of the Hg was lost, thus contaminating the surrounding environment. Extensive geochemical research regarding historical small-scale roasting sites in the Idrija surroundings determined extremely high Hg levels at these sites [39–43]. It has been estimated that about 40 tons of Hg are still present at the historical ore-roasting sites [39]. In the second half of the 17th century, the first roasting plant at Idrija was built and since then ore roasting took place in Idrija, whereas waste residues, which still contained significant Hg levels, were deposited nearby or dumped into the Idrijca River, which carried the material downstream to the Soča River and finally to the Gulf of Trieste [44–47]. In the last century of mining at Idrija, less and less rich ore was excavated, thus necessitating considerable quantities of ore. As a consequence, big new dumps of roasting residues were deposited on the riverbanks, and a large amount of waste material was dumped into the Idrijca River. During intensive ore processing, Hg was spread into the atmosphere via a rotary kiln chimney as gaseous and particulate emissions, which caused widespread soil contamination.

At present, the Hg^0 release into the atmosphere from the Idrija mining district has been estimated to be between 17 and 51 kg yr^{-1} [48,49], with high atmospheric Hg concentrations restricted to the area of the former roasting plant [50,51]. However, Hg^0 fluxes at the soil–air interface within the Idrija mining district have been estimated at only a few locations using direct measurements [49,50] or laboratory incubations [27], resulting in variable evasion rates as a function of the Hg binding phase in the soil and environmental parameters, mainly soil temperature. Therefore, the aim of this study was to broaden the spatial coverage of direct measurements of Hg^0 fluxes at the soil–air interface in the Idrija mining district. Measurements were conducted in the summer during daylight hours to detect the maximum potential Hg^0 evasion at the selected sites. Three sites within the urban area of Idrija were selected to measure the potential Hg^0 evasion in areas subject to different types and degrees of Hg contamination (low contamination, natural enrichment, and heavy contamination from atmospheric deposition from modern furnaces). Moreover, measurements were conducted at one of the historic roasting sites in the forest surrounding Idrija, for which no information exists at present regarding Hg^0 gaseous exchanges at the soil-air interface. This site provides a unique opportunity to study the Hg^0 fluxes in a heavily contaminated area several centuries after the cessation of ore roasting.

2. Materials and Methods

2.1. Environmental Settings and Experimental Sites

The town of Idrija is located 334.5 m a.s.l. on an alluvial plain in the narrow valley at the confluence of the Nikova and Idrijca Rivers, approximately 50 km west of Ljubljana. Most of the plain consists of sedimentary carbonate rocks (limestone and dolomite) with the occurrence of detrital sedimentary rocks (breccias, conglomerates, sandstones, mudstones, claystones, and shales) [37,38]. The climate of the area is warm and humid, characterised by notable precipitation (2000–3200 mm y^{-1}) distributed throughout the year [51].

For this study, 5 sites distributed within the Idrija mining district and its surroundings were selected based on existing information regarding the spatial distribution of Hg in soils [33,34,52]. Three sites were selected in the urban area of Idrija (ID1, ID2, and ID3) and two in its surroundings at the historic roasting site of Pšenk (PS1 and PS2) (Figure 1). ID1 was located in the southeastern part of Idrija just outside the urban area. This site was chosen as it is considered to be less impacted and only marginally affected by emissions related to ore processing due to its distance from the roasting locations. Conversely, ID2 was situated in the southwestern part of the urbanised area, also known as the "Pront" area, where the occurrence of Carboniferous schists containing cinnabar and native Hg has been reported [36]. Moreover, a roasting site active in the earliest years of Hg extraction (1490–1510) was located close to this area [53]. Finally, site ID3 was located in the northern part of the town near the former furnaces used during the last centuries of mining activity. These furnaces represented a significant source of atmospheric Hg, which can be transferred to the surrounding soils via wet and dry depositions [33,34,54].

Measurements were conducted at Pšenk both in an open grassland located outside the area where the roasting site is thought to have been located (PS1) and within the most contaminated area (PS2) where extremely high Hg concentrations (up to thousands of mg kg^{-1}) have been previously reported for both surface and deep soil layers. Many fragments of earthen vessels broken due to the high temperatures reached during burning were previously found in this area, confirming the occurrence of ore roasting [43,52]. In contrast to other sites, PS2 is located in a forested area dominated by Norway spruce (*Picea abies*), with an occurrence of beech (*Fagus sylvatica*) and sycamore maple (*Acer pseudoplatanus*). Consequently, a relevant amount of litter was present on the soil surface, together with mosses. Measurements at all other sites were performed under direct solar irradiation in grasslands characterised by well-developed herbaceous vegetation cover dominated by *Poaceae* and *Asteraceae* at ID1 and ID3 and by lower-height herbaceous vegetation with a more extended occurrence of *Fabaceae* at ID2.

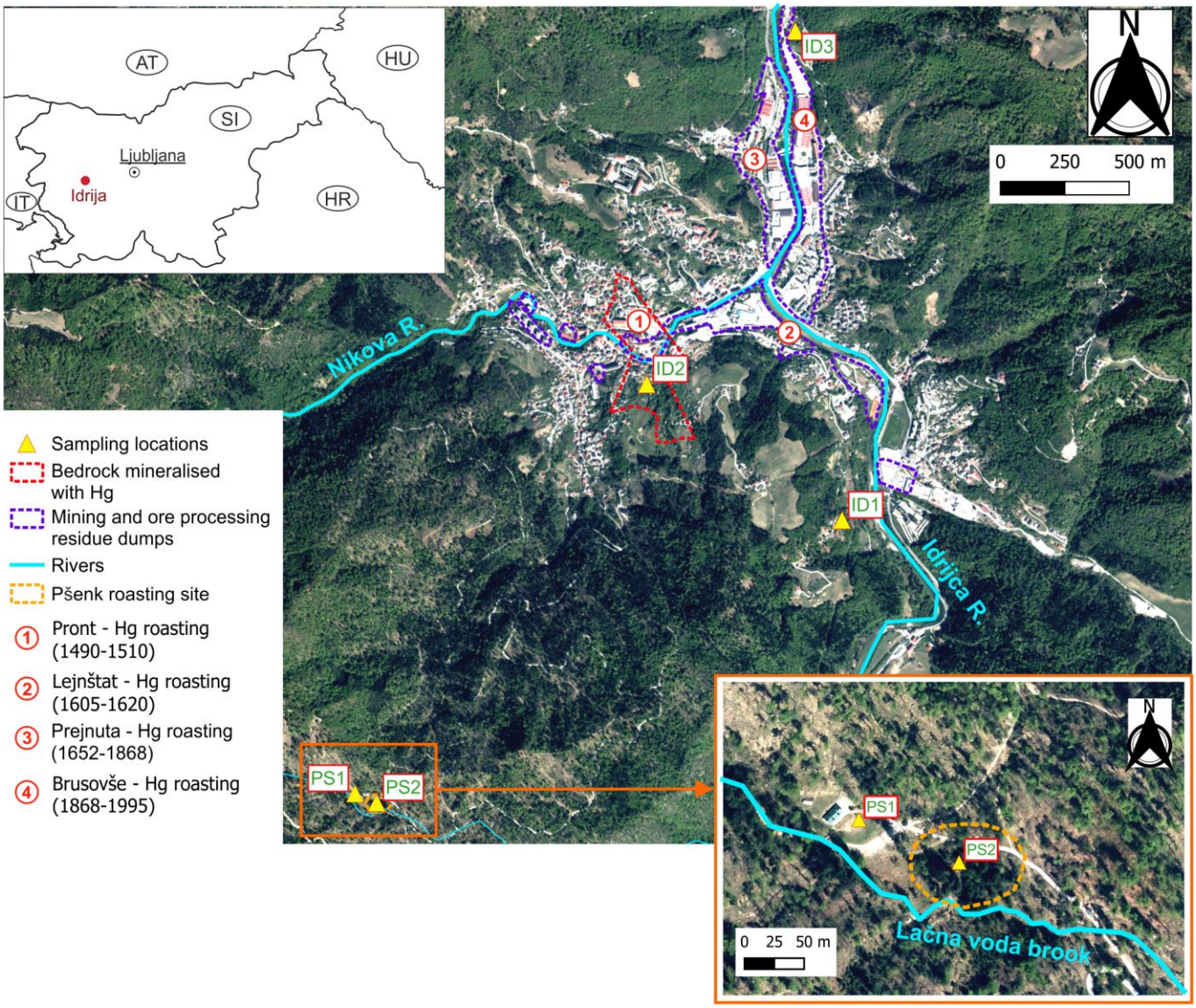

Figure 1. Study area and location of sampling sites within the town of Idrija (ID1, ID2, and ID3) and at the historic roasting site of Pšenk (PS1, PS2). The most Hg-contaminated area at Pšenk is highlighted (dotted orange circle). Modified from [34,43,55].

2.2. Field Activity

Sampling activities for the determination of Hg^0 fluxes at the soil–air interface were performed in August 2022 over a period of two days. The first was dedicated to measurements at the sites within the town of Idrija (ID1, ID2, ID3), and the second focused on the historic roasting area of Pšenk (PS1, PS2). Field measurements of Hg^0 fluxes were performed using a Plexiglas non-steady state (NSS) rectangular flux chamber ($l \times w \times h$, $60 \times 20 \times 25$ cm), as described in a previous study [56]. At each site, fluxes were measured in at least three different plots, preserving the natural vegetation cover. In order to compare the potential Hg^0 emissions under different conditions, all measurements at various locations were conducted between 12 p.m. and 3 p.m., corresponding to the period of the day when the highest evasion rates are expected [50].

Prior to the measurements, a 5 cm tall stainless-steel frame was installed at a depth of 2 cm in the soil on each plot. The chamber was then fitted onto the frame, and soil was loosely packed around the external walls to achieve an optimal seal and avoid the intrusion of external air inside the chamber [57]. During the measurements, the air was continuously

recirculated through the chamber at a constant flow rate (10 L min^{-1}) using an integrated pump from a portable Hg^0 analyser (Lumex RA-915M, Lumex, St. Petersburg, Russia) connected to the chamber in a closed circuit using two Teflon tubes attached to either end. The Lumex works via atomic absorption spectrometry with Zeeman background correction [58] and facilitates the determination of Hg^0 concentrations in the air at sampling intervals selected by the operator over a wide dynamic range. Gaseous Hg^0 concentrations in the air measured by the instrument are indeed influenced by the chosen sampling interval [59], ranging from a limit of detection of 0.3 ng m^{-3} (for an average measuring time of 30 s) or 2 ng m^{-3} (for an average measuring time of 1 s) up to a maximum of 30,000 ng m^{-3}.

In this study, the Hg^0 concentrations were recorded at a sampling rate of 1 Hz. Real-time data are visualised on the Lumex display and stored in the instrument's internal data logger.

The main advantage of the NSS chamber methodology coupled with real-time analysers is that it allows for the reliable determination of Hg^0 fluxes at the soil–air interface with short enclosure times [60,61]. Short deployment times allow one to minimise the decrease in the concentration gradient between the soil and chamber headspace, which can reduce the evasion rate [62]. This procedure also limits the alteration of the microclimatic conditions of the soil–air boundary layer caused by the chamber placement (e.g., in terms of temperature and water vapour build-up), which can affect the measured Hg^0 flux [63–65]. In this study, the sampling time for each plot was set to 5 min, during which the increase in Hg^0 concentration in the chamber headspace demonstrated a good fit for the linear regression ($R^2 \geq 0.95$). Thus, Hg^0 fluxes (F) were estimated using a linear calculation scheme according to the following equation (1) [66,67]:

$$F = \frac{dC}{dt}\frac{V}{A} \quad (1)$$

where dC/dt is the increase in Hg^0 concentrations inside the chamber estimated as the slope of the concentration versus time curve, V is the internal volume of the chamber (0.03 m^3), and A is the basal area (0.12 m^2).

Before sampling, the chamber was cleaned with diluted HNO_3 (5% v/v) and rinsed several times with ultrapure water (Milli-Q® Direct Water Purification System, Merck KGaA, Darmstadt, Germany). The experimental setup was checked in the laboratory using chamber blank measurements performed before and after each sampling day by sealing the chamber on a clean polycarbonate surface, resulting in low blank fluxes (1.6 ± 1.0 ng m^{-2} h^{-1}).

Air temperature and humidity were measured in the field using a portable thermo-hygrometer (HI9565—Hanna Instruments, Padova, Italy). Incident radiation between 250 and 400 nm was monitored during the Hg^0 flux measurements using a specific sensor (SU-420—Apogee Instruments, Logan, UT, USA) mounted near the sampling points under the same solar irradiation conditions. The soil temperature was determined in each plot during measurements at a depth of 2 cm using a thermal probe.

After the Hg^0 flux measurement, a topsoil sample (≈0–2 cm) was collected manually from each plot. This surficial soil layer is considered to be the most involved in the gaseous exchange processes of Hg in the atmosphere [68,69]. The soil samples were sealed in polyethylene bags and taken to the laboratory for subsequent determination of grain size, pH, organic matter content, total Hg concentration and Hg speciation.

2.3. Analytical Determinations

Before analysis, soil samples were carefully separated from coarse plant residues of both aboveground (stems and leaves) and belowground biomass (roots).

The grain size of the soil samples was determined using aliquots of approximately 20 g of fresh soil. After a 24 h treatment with H_2O_2 to remove most of the organic matter (OM), the samples were wet sieved at <2 mm to eliminate coarse organic residues. Analytical determination was performed on the resulting fraction using a laser granulom-

etry (Mastersizer 2000, Malvern Instruments Ltd., Worcestershire, UK) according to the ISO 13320:2020 method.

For the other determinations, soil samples were air-dried at room temperature and sieved at <2 mm. The loss on ignition (LOI) method was used at 550 °C for the determination of soil OM content [70]. Soil pH was measured using a glass electrode in a 1:2.5 soil/ultrapure water suspension after two hours of equilibration [71].

The total Hg content and Hg speciation in soils were evaluated by means of thermo-desorption technique using the Lumex Hg analyser described above coupled with a pyrolysis attachment (PYRO-915+) consisting of a double-chamber atomising system combined with a heated analytical cell [72]. Briefly, a sample in an amount ranging from 1 to 30 mg, depending on the expected Hg concentration, was weighed in a quartz boat with a built-in type K thermocouple and inserted into the attachment. The samples were then thermally decomposed via gradual heating from ambient temperature to 700 °C at a rate of ~0.5 °C s^{-1}. Depending on its chemical form, Hg is released at specific temperature intervals during heating. The progressive Hg^0 release during decomposition was visualised in real-time by the software which controls the instrumentation (Rapid ver 1.00.585). The desorption temperatures of pure Hg compounds mixed with carbonate powder obtained in a previous study [73] were used for the identification of the occurring Hg species. Due to the overlap of the desorption peaks of β-HgS and Hg bound to OM, characterised by different mobility and availability in soil, an oxidation test was performed to identify the species responsible for the Hg release in this temperature range according to the procedure described by Biester et al. [44]. Briefly, an aliquot of approximately 0.5 g of sample was treated with 0.02 M HNO_3 in centrifuge tubes and placed in a water bath at 85 °C for 2 h. Then, 4 mL of H_2O_2 was added, and the samples were heated for an additional two hours. After this period, the leached residues were washed with Milli-Q® water and dried at 55 °C for 24 h. Finally, the treated samples were analysed again using thermo-desorption. This treatment can dissolve Hg bound to OM but cannot mineralise β-HgS [54].

Total Hg concentrations in the soil samples were obtained via the integration of the subtended area of thermo-desorption curves using Rapid software. The accuracy of the method was checked via the analysis of certified reference materials (PACS-3, Hg = 2.98 ± 0.36 mg kg^{-1}, ERM-CC144, Hg = 5.90 ± 0.60 mg kg^{-1}) obtaining acceptable recoveries (89–103%).

The relative amounts of different Hg fractions were calculated by integrating the area under every single peak according to the approach described by Biester and Scholz [74].

3. Results

3.1. Soil Characteristics

Excluding the samples collected at site PS2, the soil pH ranged from neutral to slightly alkaline (6.88–7.97) showing the highest pH values at site ID2. Forest topsoil from PS2 under coniferous trees showed acidic pH values, particularly those collected in the "O" horizon in plots A and B (Table 1). In terms of grain size, these soils can be defined as loamy sand and sandy loam, respectively, according to the USDA textural classification [75], and were characterised by an extremely high OM content, as evidenced by LOI values of up to 54.6%. Conversely, the soils collected at the other location at Pšenk (PS1) and at all the sites within the town of Idrija (ID1, ID2, and ID3) showed a greater abundance of the silty fraction and were classified as silty loam. These soils presented a lower content of OM, with LOI values slightly higher at site ID3 compared to ID1 and ID2 and ranging between 6.91 (ID2-C) and 14.44% (ID3-A) (Table 1).

Table 1. Summary of the main physicochemical characteristics of soils from the investigated sites, reported as the average value of all measuring plots.

Parameter	ID1	ID2	ID3	PS1	PS2
pH	7.72 ± 0.09	7.89 ± 0.08	7.19 ± 0.50	7.75 ± 0.05	4.72 ± 1.10
LOI_{550} (%)	11.5 ± 1.0	8.88 ± 1.73	13.4 ± 1.2	11.1 ± 1.0	39.0 ± 24.8
Sand (%)	40.7 ± 3.4	34.8 ± 4.2	41.9 ± 0.7	40.3 ± 5.7	61.1 ± 18.8
Silt (%)	55.0 ± 2.9	60.9 ± 3.6	53.9 ± 0.9	54.4 ± 5.8	35.9 ± 15.8
Clay (%)	4.3 ± 0.5	4.3 ± 0.6	4.2 ± 0.3	5.3 ± 0.6	2.9 ± 3.0
THg (mg kg^{-1})	9.76 ± 2.96	166 ± 47	180 ± 46	15.7 ± 6.3	6466 ± 4119
α-HgS (%)	51.2 ± 2.0	81.5 ± 5.1	31.4 ± 7.2	59.4 ± 6.1	53.6 ± 6.0

3.2. Topsoil Total Hg Concentration and Speciation

Mercury content and speciation in the topsoils investigated in this study showed a high spatial heterogeneity due to the variable contribution of different Hg supplies in the various investigated sites, such as atmospheric depositions, direct discharges of roasting residues, losses during ore transport and processing, and natural occurrences [33]. Overall, the concentration of THg in the topsoils of all investigated sites spanned between 7.32 (ID1-B) and 10,400 mg kg^{-1} (PS2-A) (Figure 2).

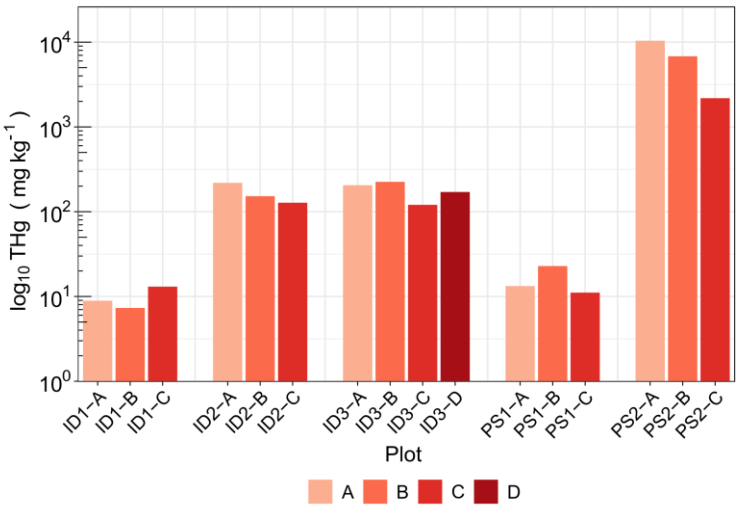

Figure 2. THg concentrations in topsoils (0–2 cm) collected after the Hg0 flux measurements directly under the chamber.

The highest THg concentrations were found at site PS2 (2184–10,400 mg kg^{-1}), corresponding to the area thought to be the historic roasting site of Pšenk, and was heavily impacted by Hg losses that occurred while it was active from the 16th to 17th centuries [39,52]. Mercury content in the topsoil sharply decreases moving away from the roasting site, resulting in significantly lower values at site PS1 (11.1–22.8 mg kg^{-1}) located a few dozen metres away and at an elevation approximately two metres higher than PS2. As expected, the lowest THg concentrations at Idrija were observed at the less impacted site ID1 (7.32–13.1 mg kg^{-1}). Conversely, the highest and comparable THg concentrations were found at ID2 (128–219 mg kg^{-1}) and ID3 (121–225 mg kg^{-1}), which are subject to more natural and/or anthropogenic supplies of this metal. Overall, these data are in good agreement with the spatial distribution of Hg concentration in the topsoils of the investigated areas reported in previous works [34,52]. Almost all samples exceeded the critical value for Hg concentration in soils established by the Slovenian legislation (10 mg kg^{-1}, Official Gazette RS 68/96) and were significantly higher than the estimated average value for European topsoils (0.055 ± 0.004 mg kg^{-1}, [76]).

The curves generated by the thermo-desorption analysis showed a double peak for all the samples, with the first release occurring between 215.9 °C and 271.8 °C and the second between 314 °C and 371.5 °C (Figure 3).

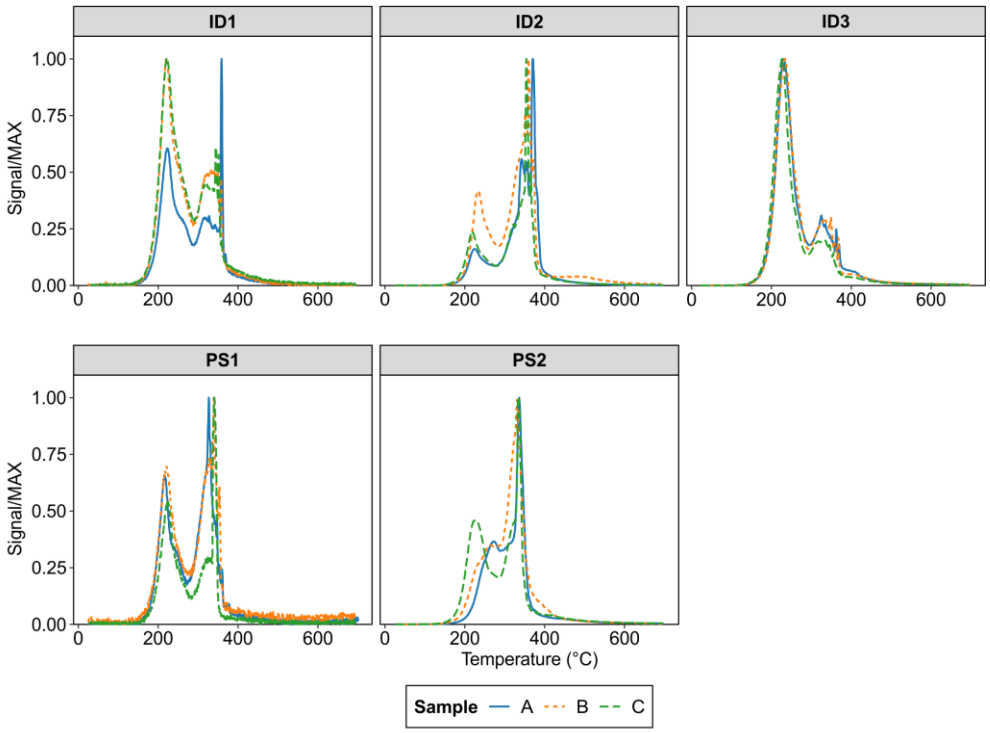

Figure 3. Thermo-desorption curves obtained from pyrolysis of soil samples from each site.

This second peak is associated with the occurrence of α-HgS (cinnabar), as the temperatures are comparable to those obtained for pure red α-HgS from Idrija [73]. Moreover, these peaks present a characteristic shape with multiple narrow peaks attributable to the sudden releases of Hg due to the breakdown of α-HgS microcrystals [44]. Conversely, in the temperature range of the first peak, defined as the no-α-HgS fraction, the desorption of various Hg forms is reported. These forms can include metacinnabar (β-HgS) or potentially more mobile species such as Hg adsorbed by functional groups of OM or mineral surfaces of iron oxyhydroxides or clay minerals [73,77–80]. The relative abundance of the two fractions varied greatly between the investigated sites, with no-α-HgS forms prevailing at site ID3 (>60%) and α-HgS dominating at site ID2 (>70%), whereas at the other sites, a slight predominance of α-HgS was detected (Figure 4).

Considering the thermo-desorption curves obtained after the oxidation test (Figure 5), the first peak was significantly reduced or even disappeared (ID1 and PS1), indicating that most of the Hg occurring in the no-α-HgS fraction in our samples were bound to OM. The residual amount of Hg desorbed at T < 300 °C can be attributed to other forms such as β-HgS, which can be formed as a by-product during the ore roasting process [81] or in contaminated soils from thiolate complexes [82], and has been previously detected in the environment at Idrija [83,84]. Subtracting this residual fraction, the relative abundance of organic-bound Hg was relatively low at ID2 (11.7–19.2%) and PS2 (17.2–28.6%), whereas the highest values were found at ID3 (57.6–72.9%).

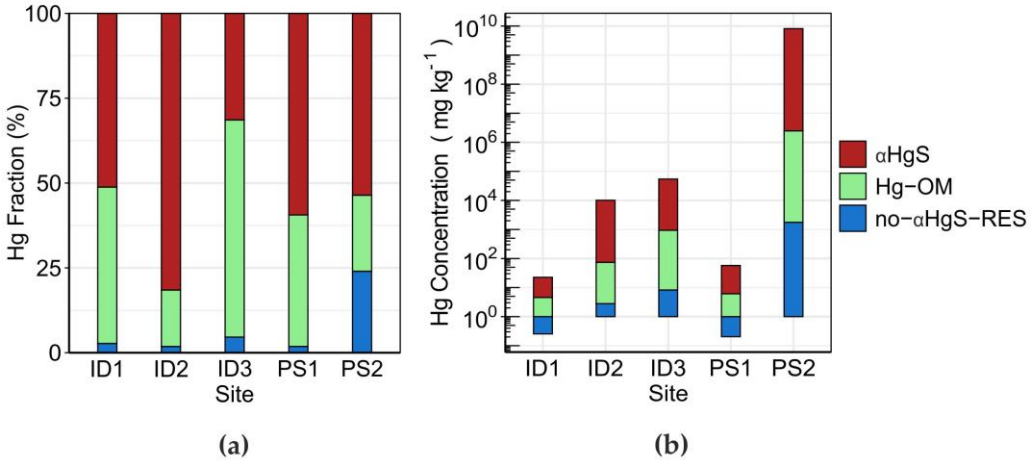

Figure 4. (**a**) Average relative abundance of α-HgS, Hg bound to OM and residual no-α-HgS after oxidation; (**b**) average Hg concentrations in the various fractions.

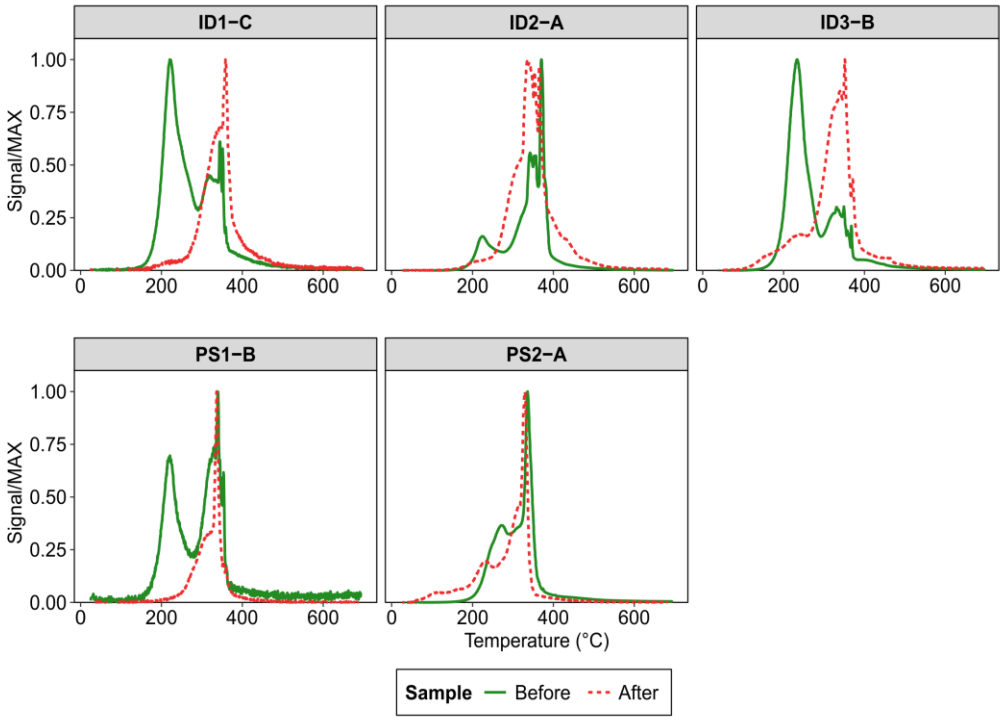

Figure 5. Comparison of Hg thermo-desorption curves before and after the oxidation test. The sample with the highest initial THg content for each site is shown.

3.3. Elemental Mercury (Hg^0) Fluxes at the Soil–Air Interface

Flux measurements were performed under mostly sunny conditions and only partially interrupted by a light cloud cover during measurements at ID1. The incident UV radiation measured near the sampling points ranged between 18.2 (ID3-C) and 36.9 W m^{-2} (PS1-B) for plots under direct solar irradiation, whereas lower values were obtained for plot PS1-C (shaded by nearby trees) and especially for measures taken at PS2 in the shaded forested area where UV radiation was relatively constant and always below 2 W m^{-2} (Table S1). Similarly, site PS2 showed the lowest air and soil temperatures (26.6 and 21.5 °C, respectively), whereas, at all other sites, air temperatures were above 30 °C and soil temperatures ranged between 24 °C and 32 °C (Table S1).

Overall, Hg^0 fluxes at the soil–air interface varied between 70.7 (ID1-B) and 2466 ng m^{-2} h^{-1} (PS2-C), with a relatively high variability even on a small spatial scale

between the different measurement plots at each site (Table S1). Taking into consideration only undisturbed plots with natural vegetation/litter cover (Figure 6), the highest emissions were, on average, recorded at site ID2 (605.4 ± 154.8 ng m^{-2} h^{-1}) in the naturally Hg enriched "Pront" area, whereas the lowest fluxes were found at the less impacted site ID1 (75.8 ± 8.2 ng m^{-2} h^{-1}).

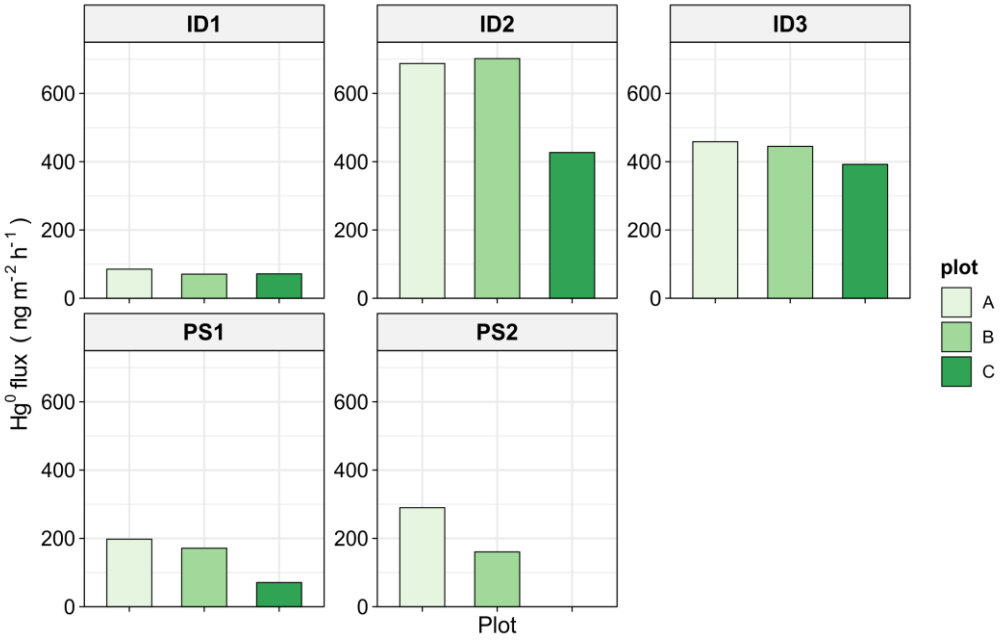

Figure 6. Hg^0 fluxes at the soil–air interface in the different plots (A, B and C) for each investigated sites, preserving the natural vegetation/litter cover.

Relatively high fluxes were also observed at ID3 near the location of the now-disused modern furnace, where the maximum value (538.2 ng m^{-2} h^{-1}) was obtained for plot D from a bare soil surface in the grassland area. In the area of the historic roasting site of Pšenk, excluding the extremely high flux recorded at PS2-C from bare soil under an uprooted tree, comparable Hg^0 emissions were recorded for sites PS1 and PS2. Slightly lower values were recorded in the first location, with the minimum corresponding to the shaded plot C where the flux was less than half of that under direct sunlight (plots A and B). Finally, at PS2, Hg^0 fluxes slightly increased in the second measurements performed on plots A and B after the removal of the litter but remained lower than those found at sites ID2 and ID3 (Table S1).

4. Discussion

The Hg^0 fluxes recorded in this study showed a relatively high spatial variability both between the different sites and within the various plots from which emissions were measured at each site. This may have been caused by the high natural heterogeneity of surface soils, even on a small spatial scale, resulting in the high variability of several characteristics (i.e., OM content, Hg concentration and speciation, pH, grain size and porosity, pH, soil cover, and soil moisture), which can differently affect Hg^0 emission at the soil–air interface [85,86]. Moreover, the environmental parameters that strongly affect Hg^0 fluxes, such as UV radiation and temperature, differed between the various investigated sites. Consequently, the magnitude of Hg^0 fluxes recorded at different sites may be influenced by complex site-specific interactions between various factors, which in turn may likely mask the variation of fluxes caused by the variation of a single factor [7,15]. As a result, poor correlations between the fluxes and various environmental parameters were found (Figure 7).

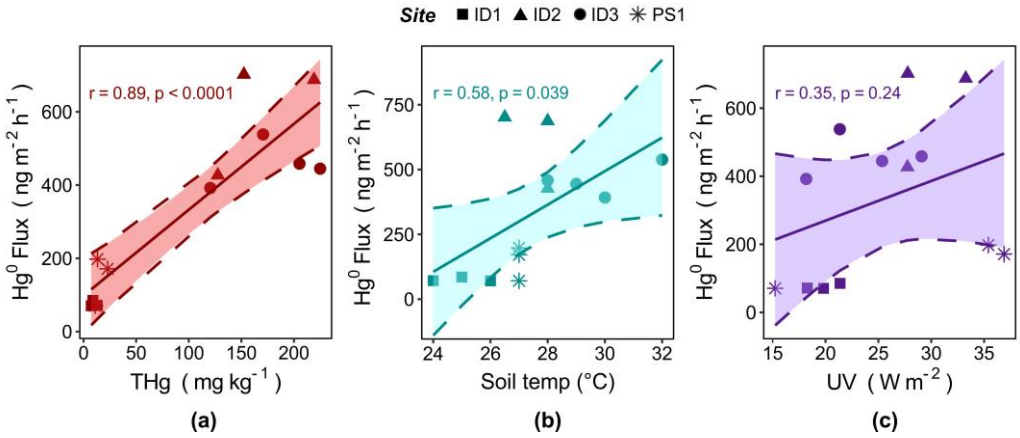

Figure 7. Relationship between Hg^0 fluxes and (**a**) THg soil concentration, (**b**) soil temperature, and (**c**) UV radiation during field measurements. Only sites under direct solar irradiation on grassland were considered.

Typically, in areas characterised by Hg-enriched substrates due to natural geology or anthropogenic inputs, one of the most important factors controlling Hg^0 fluxes at the soil–air interface is represented by the concentration of THg in the surface soil [15,87,88]. Generally, high substrate THg concentrations lead to greater availability of Hg^{2+} for reduction to volatile Hg^0 via both abiotic and biotic reactions enhanced by high temperature and sunlight [21,89]. As a result, high Hg^0 fluxes are expected from these areas due to an increased pool of Hg^0 available for volatilisation in the soil [68].

Overall, the Hg^0 fluxes observed in this study are comparable with the data reported by Agnan et al. [15] for sites contaminated by mining, although in a somewhat lower range. Fluxes of Hg^0 in the order of hundreds of ng m^{-2} h^{-1} during summer from contaminated soil surfaces near the town of Idrija have been previously predicted [49], in agreement with the results of our field measurements.

4.1. Elemental Mercury (Hg^0) Fluxes and Soil Total Hg Concentrations

Excluding site PS2, which is characterised by extremely high THg concentrations but located in a shaded forested area, an overall significant positive correlation was found between Hg^0 fluxes and soil THg concentrations (r = 0.89, $p < 0.0001$, $n = 11$) in all the other sites located in open grasslands (Figure 7). This confirms the importance of Hg availability in the substrate in influencing the amount of Hg^0 released into the atmosphere. Accordingly, in this study, the highest average Hg^0 fluxes were recorded at sites ID2 and ID3 (Figure 8), characterised by the highest THg concentrations (excluding PS2). These emissions are significantly higher than those previously obtained with the same experimental setup used in this study for grassland soil surfaces of the Isonzo River alluvial plain in summer (range = 62.4–345 ng m^{-2} h^{-1}, [56]), impacted by Hg transported by river sediments in the same drainage basin downstream of the Idrija mining district. Mercury content in soils from the Isonzo River plain investigated in the above-mentioned study was significantly lower (range = 2.22–25.33 mg kg^{-1}, [56]) than that of soils from sites ID2 and ID3. In contrast, sites ID1 and PS1 were characterised by the lowest values of both THg concentrations in topsoils and Hg^0 fluxes, but comparable with those found in the downstream Isonzo alluvial plain [56]. These findings further confirm the importance of Hg content in the substrate to support its release into the atmosphere.

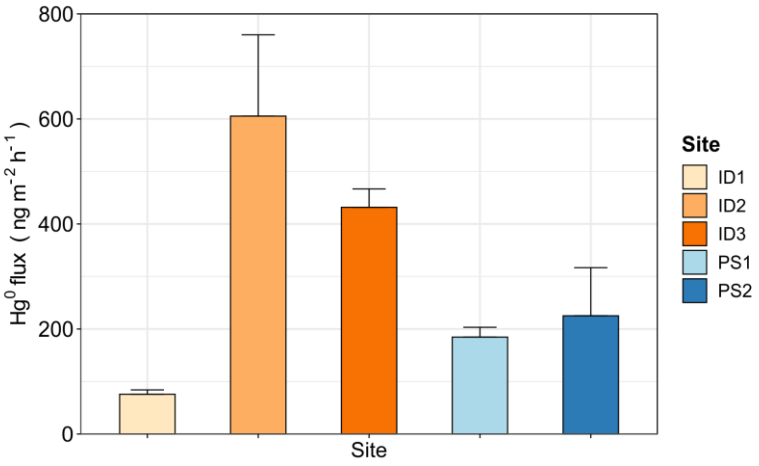

Figure 8. Average Hg^0 fluxes at the soil–air interface at various sites. Only plots with natural vegetation/litter cover were considered for calculation.

4.2. Elemental Mercury (Hg^0) Fluxes and Hg Speciation in Soil

Interestingly, Hg^0 fluxes at ID3 are relatively lower than those recorded at ID2 despite a slightly higher THg content in the topsoils and the different Hg speciation, which can strongly affect the mobility of this element in the environment [90]. Compared to many other metals, Hg tends to be relatively immobile in soils [91]. In mining and naturally enriched areas, the most common Hg form is usually represented by α-HgS, which is extremely insoluble and subsequently scarcely available for transformation compared to other species [27,92]. Conversely, in areas affected by Hg supplies mainly via atmospheric depositions, Hg^{2+} arriving in the soil can be readily adsorbed by OM due to its high affinity for reduced sulphur groups or mineral soil surfaces, forming stable complexes [93,94]. The thermo-speciation results obtained in this study are in agreement with this hypothesis, showing a predominance of α-HgS at ID2 located in the naturally Hg-enriched "Pront" area and the highest abundance of organic-bound Hg at ID3, likely heavily impacted by atmospheric depositions of Hg emitted by the nearby roasting plant that is now disused. Indeed, most of the Hg derived from atmospheric depositions is usually retained in the upper soil horizons owing to adsorption by OM [54,93,95]. Some α-HgS is also present in the topsoil at site ID3, likely as a result of the dispersion of dust from the roasting plant, which can include small particles of this mineral [33].

Mercury adsorbed on mineral and organic soil surfaces needs to be desorbed in order to be reduced to Hg^0 available for volatilisation [68,96]. This process and its subsequent reduction to volatile Hg^0 are catalysed by solar irradiation and high temperatures [97].

Generally, soils enriched in α-HgS must absorb more energy to initiate Hg^0 emission compared to those dominated by other Hg forms, resulting in lower light-enhanced emission [98,99]. Our results seem to be in contrast with this rule, as higher Hg^0 fluxes may be expected at ID3 than at ID2, considering the greater abundance of no-α-HgS forms (mostly OM-bound Hg, as shown in Figure 4). However, the soil at ID2 overlies rocks containing both α-HgS and native Hg [34,36], and previous studies have reported the occurrence of Hg^0 in a tailing sample collected nearby [83]. Elemental Hg represents the most easily volatilised form [27] but was not detected via the thermo-desorption technique. However, its occurrence in quantities that are too low to be detectable at ID2 cannot be excluded and may help explain the high fluxes recorded at this site. On the contrary, the complexation of Hg derived from atmospheric deposition by OM can favour the migration of the most available forms of the pollutant to deeper soil layers [43,77,91,100], making it less available for re-emission into the atmosphere [95]. This may be in agreement with the higher concentrations of water-soluble Hg detected in deeper soil layers in the area subject to strong atmospheric supplies of Hg at Idrija [101].

4.3. Elemental Mercury (Hg^0) Fluxes and Meteorological Parameters

Solar radiation and soil temperatures can exert a synergic control on Hg^0 fluxes as incident radiation heats the soil, resulting in increased desorption and diffusion of Hg in the soil solution and pore space air due to increased thermal motion [27,92,102]. Higher temperatures can also catalyse the reaction rates of the abiotic and biotic reduction of Hg^{2+} [96]. In contrast, incident radiation, mostly at UV wavelengths, can also independently promote the formation of Hg^0 on soil surfaces via photoreduction [103].

The different UV irradiation may explain the lower Hg^0 fluxes recorded at ID3 than at ID2. The lower UV irradiation found at ID3 may have resulted in less Hg^0 formation via photoreduction. It has indeed been reported that rapid changes in UV radiation can strongly affect the magnitude of Hg^0 fluxes at the soil–air interface [24]. Previous measurements conducted near sampling site ID3 over the entire 24 h period found an average emission of 84.4 ng m^{-2} h^{-1} [50]. This value was lower than those found in our study and was influenced by the low emissions recorded overnight, indicating that in the absence of radiation and at lower temperatures, Hg^0 fluxes into the atmosphere are suppressed. At a second location about 40 km downstream from the town of Idrija, the fluxes measured were even lower (34 ng m^{-2} h^{-1}, [50]) due to the reduced influence of mining activities, as evidenced by the lower Hg content in the soil.

The combined effect of UV radiation and soil temperature on Hg^0 fluxes can also be confirmed by the results obtained at ID1 and PS1. [56]. The low THg concentrations found at these sites suggest that they were only marginally affected by direct Hg supplies related to mining and ore roasting, whereas they were likely to be more influenced by atmospheric depositions. This hypothesis is supported by the fact that almost all the no-α-HgS fraction can be attributed to organic-bound Hg since, after the oxidation test, the first Hg desorption peak disappeared (Figure 5) [54]. As stated above, organic-bound Hg is usually the dominant form of this metal in atmospherically influenced areas [95], whereas the occurrence of α-HgS can be attributed to the wind transport of HgS-bearing dust particles [33,52]. However, despite the similar Hg concentrations and speciation at these two sites, Hg^0 fluxes were lower at ID1, likely due to the light cloud cover encountered during sampling at this site, which caused lower UV radiation and soil temperatures than at PS1.

4.4. Elemental Mercury (Hg^0) Fluxes and Vegetation Cover

The formation and volatilisation of Hg^0 are often limited in soils covered by a developed continuous herbaceous vegetation in comparison with bare soil surfaces due to shading [56,64,104], even in heavily contaminated mining districts [18,21]. Considering sites ID2 and ID3, the effect of decreased UV radiation on Hg^0 fluxes at the latter site may have been enhanced by the more developed grass vegetation cover, together with the presence of a layer of dead biomass on the soil surface. The same situation was observed when comparing sites PS1 and ID1, with less developed vegetation at the former site coupled with higher fluxes. Moreover, at ID3, the highest emissions were observed in plot D, characterised by the absence of vegetation cover and consequently subject to higher direct irradiation and heating, which may have favoured the formation of Hg^0.

The importance of soil cover by vegetation in limiting Hg^0 fluxes is even more evident considering the relatively low emissions recorded at site PS2 (plots A and B), coinciding with the historic roasting site of Pšenk in a forested area. Despite a Hg concentration three orders of magnitude higher at PS2 than that found at the margins of the roasting area (PS1), the Hg^0 fluxes at these two sites were comparable. Forest ecosystems, particularly evergreen coniferous forests such as those present at PS2, are usually characterised by low Hg^0 emissions from soils due to intense canopy shading, which limits direct irradiation and heating of the soil [105,106]. This was also confirmed in our study by the nearly null UV radiation and the lowest soil temperatures recorded at this site. Under these conditions, the contribution of α-HgS can also be considered scarce due to the high activation energy required to initiate Hg^0 volatilisation [27]. However, despite shading, incident radiation

can still influence Hg^0 fluxes at the soil–air interface [23], as confirmed by the increase observed in measurements performed after the removal of the litter on plots PS2-A and PS2-B (Figure 9). These findings suggest that shading by trees is effective in limiting Hg^0 evasion at the soil–air interface, even in highly contaminated soils under investigation.

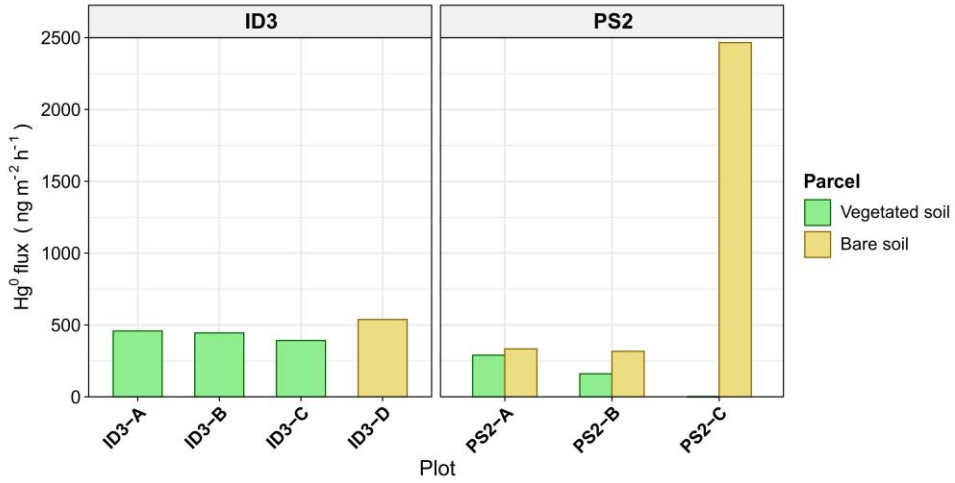

Figure 9. Hg^0 fluxes recorded from soils with and without vegetation (ID3) and litter cover (PS2). Measurements on plots PS2-A and PS2-B were conducted before and after the removal of the litter.

Another aspect to be considered is the length of time that has passed since the strong Hg inputs in the historic roasting area. Although it was assumed that other than atmospheric emissions, large amounts of Hg^0 were lost in the environment either via spillage or in roasted residues directly discharged into the soil [52], it is possible that this species escaped into the atmosphere or was oxidised and then bound to OM, a process that can quickly occur in oxidised soil layers [107,108]. Moreover, oxidised Hg bound to the more soluble fraction of the OM may have leached to deeper soil layers [43]. Considering that this fraction of Hg is generally believed to be more available, it cannot be excluded that Hg^0 produced in-depth via dark reduction processes [23,93,109] is then re-adsorbed by the abundant OM in the surface layer constantly provided by the renewal of forest vegetation, limiting its diffusion into the atmosphere [68,110,111]. This process may have been further favoured by the acidic soil pH characteristics of coniferous stands due to decreased OM solubility, confirming that these ecosystems can retain high amounts of Hg in their organic soil layers [112–114]. Moreover, Hg^{2+} reduction seems to decrease with decreasing pH [92,115], limiting Hg^0 fluxes at PS2. Finally, the long-term burial of wastes containing Hg in organic-rich soils, such as those occurring at PS2, could favour the formation of more stable and less mobile Hg forms, such as β-HgS [82,116]. The occurrence of other Hg forms at PS2 can be confirmed by the lower decrease in the first desorption peak after the oxidation test compared to the other samples (Figure 5).

The significant limitation of Hg^0 fluxes caused by shading by trees was highlighted by the extremely high Hg^0 flux recorded from PS2-C (2466 ng m^{-2} h^{-1}) under a recently uprooted tree. The topsoil from this plot was characterised by a lower Hg and OM content than other measuring points at PS2 and by the complete absence of litter on the soil surface, resulting in conditions more conducive to Hg^0 evasion. This result gives an indication of the potential Hg^0 emissions from this site in the absence of the forest, suggesting that preserving the current ecosystem can effectively help naturally mitigate the re-emission of Hg^0 from these heavily contaminated soils and its further atmospheric dispersion. Previous studies have indeed shown that removal of the forest results in a sudden increase in Hg^0 fluxes [117,118], which, considering the extremely high Hg content of these soils, may lead to the occurrence of high local levels of atmospheric Hg^0.

5. Conclusions

The results of field measurements of Hg^0 fluxes at the soil–air interface presented in this study provide new data on the mobility of Hg between terrestrial and atmospheric compartments at contaminated sites within the Idrija Hg mining district. The main findings of this study are summarised as follows:

- Measured Hg^0 fluxes showed great spatial variability.
- The release of Hg^0 into the atmosphere depends on complex site-specific interactions between possible influencing factors.
- Considering measurements conducted on grasslands under direct solar irradiation, the total topsoil Hg content can be considered the main driver of Hg^0 evasion.
- Gaseous Hg^0 fluxes increase under high UV radiation and soil temperature, which in turn can increase the rate of Hg reduction reactions.
- Well-developed herbaceous vegetation can strongly limit Hg^0 evasion from contaminated soil due to surface shading. This is confirmed by the increase in Hg^0 fluxes observed from bare soil plots compared with vegetated plots and by relatively low Hg^0 fluxes from shaded locations found at the extremely contaminated historic roasting site.
- Forests can significantly reduce the impact of heavy soil contamination in the local atmosphere. However, care should be taken in forest management practices, as clear-cut forests may expose contaminated soils to direct solar radiation, potentially resulting in high Hg^0 emissions.

The results reported in this study highlight that the measurements conducted using the non-steady state chamber approach are extremely sensitive to varying environmental conditions. Due to the portability of the instrumentation used and the short time required for the measurements, these preliminary indications suggest that future work should be devoted to increasing the number of measurement sites sampled under relatively homogeneous weather conditions.

Supplementary Materials: The following supporting information can be downloaded at: https://www.mdpi.com/article/10.3390/atmos14061036/s1, Table S1: Summary of Hg content in soils, calculated Hg^0 fluxes at the soil–air interface, and main meteorological parameters recorded during sampling on all measuring plots.

Author Contributions: Conceptualization, F.F., M.G. and S.C.; methodology, F.F. and S.C.; validation, E.P. and M.G.; formal analysis, F.F. and S.C.; investigation, F.F., E.P., M.G. and S.C.; resources, E.P. and S.C.; data curation, F.F., E.P. and S.C.; writing—original draft preparation, F.F., E.P., M.G. and S.C.; writing—review and editing, F.F., E.P., M.G. and S.C.; visualization, F.F.; supervision, M.G. and S.C.; project administration, S.C. All authors have read and agreed to the published version of the manuscript.

Funding: The presented study was co-funded by the Slovenian Research Agency (ARRS) in the frame of the research programme "Groundwater and Geochemistry" (P1-0020).

Institutional Review Board Statement: Not applicable.

Informed Consent Statement: Not applicable.

Data Availability Statement: The data presented in this study are available upon request from the corresponding author.

Acknowledgments: The authors are grateful to Tatjana Dizdarevič for her kind hospitality and assistance during sampling. We warmly thank Karry Close for proofreading the manuscript. Three anonymous reviewers are greatly acknowledged for their useful suggestions, which improved the early version of the manuscript.

Conflicts of Interest: The authors declare no conflict of interest.

References

1. Gosar, M.; Teršič, T. Environmental Geochemistry Studies in the Area of Idrija Mercury Mine, Slovenia. *Environ. Geochem. Health* **2012**, *34*, 27–41. [CrossRef]
2. Martínez-Coronado, A.; Oyarzun, R.; Esbrí, J.M.; Llanos, W.; Higueras, P. Sampling High to Extremely High Hg Concentrations at the Cerco de Almadenejos, Almadén Mining District (Spain): The Old Metallurgical Precinct (1794 to 1861AD) and Surrounding Areas. *J. Geochem. Explor.* **2011**, *109*, 70–77. [CrossRef]
3. Rimondi, V.; Gray, J.E.; Costagliola, P.; Vaselli, O.; Lattanzi, P. Concentration, Distribution, and Translocation of Mercury and Methylmercury in Mine-Waste, Sediment, Soil, Water, and Fish Collected near the Abbadia San Salvatore Mercury Mine, Monte Amiata District, Italy. *Sci. Total Environ.* **2012**, *414*, 318–327. [CrossRef]
4. Clarkson, T.W.; Magos, L. The Toxicology of Mercury and Its Chemical Compounds. *Crit. Rev. Toxicol.* **2006**, *36*, 609–662. [CrossRef]
5. Rice, K.M.; Walker, E.M.; Wu, M.; Gillette, C.; Blough, E.R. Environmental Mercury and Its Toxic Effects. *J. Prev. Med. Public Health* **2014**, *47*, 74–83. [CrossRef]
6. Raj, D.; Maiti, S.K. Sources, Toxicity, and Remediation of Mercury: An Essence Review. *Environ. Monit. Assess.* **2019**, *191*, 566. [CrossRef]
7. Beckers, F.; Rinklebe, J. Cycling of Mercury in the Environment: Sources, Fate, and Human Health Implications: A Review. *Crit. Rev. Environ. Sci. Technol.* **2017**, *47*, 693–794. [CrossRef]
8. Yu, B.; Fu, X.; Yin, R.; Zhang, H.; Wang, X.; Lin, C.J.; Wu, C.; Zhang, Y.; He, N.; Fu, P.; et al. Isotopic Composition of Atmospheric Mercury in China: New Evidence for Sources and Transformation Processes in Air and in Vegetation. *Environ. Sci. Technol.* **2016**, *50*, 9362–9369. [CrossRef]
9. Cheng, I.; Zhang, L.; Mao, H.; Blanchard, P.; Tordon, R.; Dalziel, J. Seasonal and Diurnal Patterns of Speciated Atmospheric Mercury at a Coastal-Rural and a Coastal-Urban Site. *Atmos. Environ.* **2014**, *82*, 193–205. [CrossRef]
10. Schroeder, W.H.; Munthe, J. Atmospheric Mercury-An Overview. *Atmos. Environ.* **1998**, *32*, 809–822. [CrossRef]
11. Lindberg, S.; Bullock, R.; Ebinghaus, R.; Engstrom, D.; Feng, X.; Fitzgerald, W.; Pirrone, N.; Prestbo, E.; Seigneur, C. A Synthesis of Progress and Uncertainties in Attributing the Sources of Mercury in Deposition. *Ambio* **2007**, *36*, 19–32. [CrossRef]
12. Fitzgerald, W.F.; Engstrom, D.R.; Mason, R.P.; Nater, E.A. The Case for Atmospheric Mercury Contamination in Remote Areas. *Environ. Sci. Technol.* **1998**, *32*, 1–7. [CrossRef]
13. Kalinchuk, V.V.; Mishukov, V.F.; Astakhov, A.S. Arctic Source for Elevated Atmospheric Mercury (Hg0) in the Western Bering Sea in the Summer of 2013. *J. Environ. Sci.* **2018**, *68*, 114–121. [CrossRef]
14. Rolison, J.M.; Landing, W.M.; Luke, W.; Cohen, M.; Salters, V.J.M. Isotopic Composition of Species-Specific Atmospheric Hg in a Coastal Environment. *Chem. Geol.* **2013**, *336*, 37–49. [CrossRef]
15. Agnan, Y.; Le Dantec, T.; Moore, C.W.; Edwards, G.C.; Obrist, D. New Constraints on Terrestrial Surface-Atmosphere Fluxes of Gaseous Elemental Mercury Using a Global Database. *Environ. Sci. Technol.* **2016**, *50*, 507–524. [CrossRef]
16. Selin, H.; Keane, S.E.; Wang, S.; Selin, N.E.; Davis, K.; Bally, D. Linking Science and Policy to Support the Implementation of the Minamata Convention on Mercury. *Ambio* **2018**, *47*, 198–215. [CrossRef]
17. Gustin, M.S.; Coolbaugh, M.F.; Engle, M.A.; Fitzgerald, B.C.; Keislar, R.E.; Lindberg, S.E.; Nacht, D.M.; Quashnick, J.; Rytuba, J.J.; Sladek, C.; et al. Atmospheric Mercury Emissions from Mine Wastes and Surrounding Geologically Enriched Terrains. *Environ. Geol.* **2003**, *43*, 339–351. [CrossRef]
18. Fantozzi, L.; Ferrara, R.; Dini, F.; Tamburello, L.; Pirrone, N.; Sprovieri, F. Study on the Reduction of Atmospheric Mercury Emissions from Mine Waste Enriched Soils through Native Grass Cover in the Mt. Amiata Region of Italy. *Environ. Res.* **2013**, *125*, 69–74. [CrossRef]
19. Ferrara, R.; Maserti, B.E.; Andersson, M.; Edner, H.; Ragnarson, P.; Svanberg, S.; Hernandez, A. Atmospheric Mercury Concentrations and Fluxes in the Almaden District (Spain). *Atmos. Environ.* **1998**, *32*, 3897–3904. [CrossRef]
20. Huremović, J.; Horvat, M.; Kotnik, J.; Kocman, D.; Žižek, S.; Ribeiro Guevara, S.; Muhić-Šarac, T.; Memić, M. Characterization of Mercury Contamination Surrounding a Chloralkali Production Facility in Tuzla, Bosnia and Herzegovina. *Anal. Lett.* **2017**, *50*, 1049–1064. [CrossRef]
21. Wang, S.; Feng, X.; Qiu, G.; Wei, Z.; Xiao, T. Mercury Emission to Atmosphere from Lanmuchang Hg-Tl Mining Area, Southwestern Guizhou, China. *Atmos. Environ.* **2005**, *39*, 7459–7473. [CrossRef]
22. Kocman, D.; Horvat, M.; Pirrone, N.; Cinnirella, S. Contribution of Contaminated Sites to the Global Mercury Budget. *Environ. Res.* **2013**, *125*, 160–170. [CrossRef]
23. Osterwalder, S.; Huang, J.H.; Shetaya, W.H.; Agnan, Y.; Frossard, A.; Frey, B.; Alewell, C.; Kretzschmar, R.; Biester, H.; Obrist, D. Mercury Emission from Industrially Contaminated Soils in Relation to Chemical, Microbial, and Meteorological Factors. *Environ. Pollut.* **2019**, *250*, 944–952. [CrossRef]
24. García-Sánchez, A.; Contreras, F.; Adams, M.; Santos, F. Atmospheric Mercury Emissions from Polluted Gold Mining Areas (Venezuela). *Environ. Geochem. Health* **2006**, *28*, 529–540. [CrossRef]
25. Cabassi, J.; Lazzaroni, M.; Giannini, L.; Mariottini, D.; Nisi, B.; Rappuoli, D.; Vaselli, O. Continuous and near Real-Time Measurements of Gaseous Elemental Mercury (GEM) from an Unmanned Aerial Vehicle: A New Approach to Investigate the 3D Distribution of GEM in the Lower Atmosphere. *Chemosphere* **2022**, *288*, 132547. [CrossRef]

26. Floreani, F.; Acquavita, A.; Barago, N.; Klun, K.; Faganeli, J.; Covelli, S. Gaseous Mercury Exchange from Water—Air Interface in Differently Impacted Freshwater Environments. *Int. J. Environ. Res. Public Health* **2022**, *19*, 8149. [CrossRef]
27. Kocman, D.; Horvat, M. A Laboratory Based Experimental Study of Mercury Emission from Contaminated Soils in the River Idrijca Catchment. *Atmos. Chem. Phys.* **2010**, *10*, 1417–1426. [CrossRef]
28. Shi, T.; Gong, Y.; Ma, J.; Wu, H.; Yang, S.; Ju, T.; Qu, Y.; Liu, L. Soil-Air Exchange of Mercury from Agricultural Fields in Zhejiang, East China: Seasonal Variations, Influence Factors, and Models of Fluxes. *Chemosphere* **2020**, *249*, 126063. [CrossRef]
29. Wallschläger, D.; Turner, R.R.; London, J.; Ebinghaus, R.; Kock, H.H.; Sommar, J.; Xiao, Z. Factors Affecting the Measurement of Mercury Emissions from Soils with Flux Chambers. *J. Geophys. Res. Atmos.* **1999**, *104*, 21859–21871. [CrossRef]
30. Song, X.; Van Heyst, B. Volatilization of Mercury from Soils in Response to Simulated Precipitation. *Atmos. Environ.* **2005**, *39*, 7494–7505. [CrossRef]
31. Gosar, M.; Šajn, R.; Miler, M.; Burger, A.; Bavec, S. Overview of Existing Information on Important Closed (or in Closing Phase) and Abandoned Mining Waste Sites and Related Mines in Slovenia. *Geologija* **2020**, *63*, 221–250. [CrossRef]
32. Gosar, M.; Šajn, R. Mercury in Soil and Attic Dust as a Reflection of Idrija Mining and Mineralization (Slovenia) (Živo Srebro v Tleh in Podstrešnem Prahu v Idriji in Okolici Kot Posledica Orudenja in Rudarjenja). *Geologija* **2001**, *44*, 137–159.
33. Gosar, M.; Šajn, R.; Biester, H. Binding of Mercury in Soils and Attic Dust in the Idrija Mercury Mine Area (Slovenia). *Sci. Total Environ.* **2006**, *369*, 150–162. [CrossRef] [PubMed]
34. Bavec, Š.; Gosar, M.; Biester, H.; Grčman, H. Geochemical Investigation of Mercury and Other Elements in Urban Soil of Idrija (Slovenia). *J. Geochem. Explor.* **2015**, *154*, 213–223. [CrossRef]
35. Bavec, Š.; Gosar, M.; Miler, M.; Biester, H. Geochemical Investigation of Potentially Harmful Elements in Household Dust from a Mercury-Contaminated Site, the Town of Idrija (Slovenia). *Environ. Geochem. Health* **2017**, *39*, 443–465. [CrossRef]
36. Čar, J. Mineralized Rocks and Ore Residues in the Idrija Region. In Proceedings of the Meeting of Researchers Entitled: Idrija as a Natural and Anthropogenic Laboratory, Mercury as a Global Pollutant, Idrija, Slovenia, 24 May 1996; pp. 10–15.
37. Čar, J. *Geological Structure of the Idrija—Cerkljansko Hills: Explanatory Book to the Geological Map of the Idrija—Cerkljansko Hills between Stopnik and Rovte 1:25.000*; Geološki Zavod Slovenije: Ljubljana, Slovenia, 2010.
38. Mlakar, I.; Čar, J. *Geological Map of the Idrija—Cerkljansko Hills Between Stopnik and Rovte 1:25.000*; Geološki Zavod Slovenije: Ljubljana, Slovenia, 2009.
39. Gosar, M.; Čar, J. Vpliv Žgalnic Živosrebrove Rude Iz 16. in 17. Stoletja Na Razširjenost Živega Srebra v Okolici Idrije [Influence of Mercury Ore Roasting Sites from 16th and 17th Century on the Mercury Dispersion in Surroundings of Idrija]. *Geologija* **2006**, *49*, 91–101. [CrossRef]
40. Gosar, M.; Teršič, T. Contaminated Sediment Loads from Ancient Mercury Ore Roasting Sites, Idrija Area, Slovenia. *J. Geochem. Explor.* **2015**, *149*, 97–105. [CrossRef]
41. Teršič, T.; Gosar, M. Preliminary Results of Detailed Geochemical Study of Mercury at the Ancient Ore Roasting Site Pšenk (Idrija Area, Slovenia). *Geologija* **2009**, *52*, 79–86. [CrossRef]
42. Teršič, T.; Gosar, M.; Biester, H. Distribution and Speciation of Mercury in Soil in the Area of an Ancient Mercury Ore Roasting Site, Frbejžene Trate (Idrija Area, Slovenia). *J. Geochem. Explor.* **2011**, *110*, 136–145. [CrossRef]
43. Teršič, T.; Biester, H.; Gosar, M. Leaching of Mercury from Soils at Extremely Contaminated Historical Roasting Sites (Idrija Area, Slovenia). *Geoderma* **2014**, *226–227*, 213–222. [CrossRef]
44. Biester, H.; Gosar, M.; Covelli, S. Mercury Speciation in Sediments Affected by Dumped Mining Residues in the Drainage Area of the Idrija Mercury Mine, Slovenia. *Environ. Sci. Technol.* **2000**, *34*, 3330–3336. [CrossRef]
45. Gosar, M. Mercury in River Sediments, Floodplains and Plants Growing Thereon in Drainage Area of Idrija Mine, Slovenia. *Pol. J. Environ. Stud.* **2008**, *17*, 227–236. [CrossRef]
46. Covelli, S.; Faganeli, J.; Horvat, M.; Brambati, A. Mercury Contamination of Coastal Sediments as the Result of Long-Term Cinnabar Mining Activity (Gulf of Trieste, Northern Adriatic Sea). *Appl. Geochem.* **2001**, *16*, 541–558. [CrossRef]
47. Horvat, M.; Covelli, S.; Faganeli, J.; Logar, M.; Mandić, V.; Rajar, R.; Širca, A.; Žagar, D. Mercury in Contaminated Coastal Environments; a Case Study: The Gulf of Trieste. *Sci. Total Environ.* **1999**, *237–238*, 43–56. [CrossRef] [PubMed]
48. Grönlund, R.; Edner, H.; Svanberg, S.; Kotnik, J.; Horvat, M. Mercury Emissions from the Idrija Mercury Mine Measured by Differential Absorption Lidar Techniques and a Point Monitoring Absorption Spectrometer. *Atmos. Environ.* **2005**, *39*, 4067–4074. [CrossRef]
49. Kocman, D.; Horvat, M. Non-Point Source Mercury Emission from the Idrija Hg-Mine Region: GIS Mercury Emission Model. *J. Environ. Manag.* **2011**, *92*, 2038–2046. [CrossRef] [PubMed]
50. Kotnik, J.; Horvat, M.; Dizdarevič, T. Current and Past Mercury Distribution in Air over the Idrija Hg Mine Region, Slovenia. *Atmos. Environ.* **2005**, *39*, 7570–7579. [CrossRef]
51. Kocman, D.; Vreča, P.; Fajon, V.; Horvat, M. Atmospheric Distribution and Deposition of Mercury in the Idrija Hg Mine Region, Slovenia. *Environ. Res.* **2011**, *111*, 1–9. [CrossRef]
52. Teršič, T.; Gosar, M.; Biester, H. Environmental Impact of Ancient Small-Scale Mercury Ore Processing at Pšenk on Soil (Idrija Area, Slovenia). *Appl. Geochem.* **2011**, *26*, 1867–1876. [CrossRef]
53. Bavec, Š.; Biester, H.; Gosar, M. Urban Sediment Contamination in a Former Hg Mining District, Idrija, Slovenia. *Environ. Geochem. Health* **2014**, *36*, 427–439. [CrossRef]

54. Baptista-Salazar, C.; Richard, J.H.; Horf, M.; Rejc, M.; Gosar, M.; Biester, H. Grain-Size Dependence of Mercury Speciation in River Suspended Matter, Sediments and Soils in a Mercury Mining Area at Varying Hydrological Conditions. *Appl. Geochem.* **2017**, *81*, 132–142. [CrossRef]
55. Zupančič, M.; Šušteršič, M.; Bavec, Š.; Gosar, M. Oral and Inhalation Bioaccessibility of Potentially Toxic Elements in Household Dust from Former Hg Mining District, Idrija, Slovenia. *Environ. Geochem. Health* **2021**, *43*, 3505–3531. [CrossRef] [PubMed]
56. Floreani, F.; Zappella, V.; Faganeli, J.; Covelli, S. Gaseous Mercury Evasion from Bare and Grass-Covered Soils Contaminated by Mining and Ore Roasting (Isonzo River Alluvial Plain, Northeastern Italy). *Environ. Pollut.* **2023**, *318*, 120921. [CrossRef]
57. Gillis, A.; Miller, D.R. Some Potential Errors in the Measurement of Mercury Gas Exchange at the Soil Surface Using a Dynamic Flux Chamber. *Sci. Total Environ.* **2000**, *260*, 181–189. [CrossRef]
58. Sholupov, S.; Pogarev, S.; Ryzhov, V. Zeeman Atomic Absorption Spectrometer RA-915 + for Direct Determination of Mercury in Air and Complex Matrix Samples. *Fuel Process. Technol.* **2004**, *85*, 473–485. [CrossRef]
59. Mashyanov, N.; Obolkin, V.; Pogarev, S.; Ryzhov, V.; Sholupov, S.; Potemkin, V.; Molozhnikova, E.; Khodzher, T. Air Mercury Monitoring at the Baikal Area. *Atmosphere* **2021**, *12*, 807. [CrossRef]
60. Kandel, T.P.; Lærke, P.E.; Elsgaard, L. Effect of Chamber Enclosure Time on Soil Respiration Flux: A Comparison of Linear and Non-Linear Flux Calculation Methods. *Atmos. Environ.* **2016**, *141*, 245–254. [CrossRef]
61. Maier, M.; Weber, T.K.D.; Fiedler, J.; Fuß, R.; Glatzel, S.; Huth, V.; Jordan, S.; Jurasinski, G.; Kutzbach, L.; Schäfer, K.; et al. Introduction of a Guideline for Measurements of Greenhouse Gas Fluxes from Soils Using Non-Steady-State Chambers. *J. Plant Nutr. Soil Sci.* **2022**, *185*, 447–461. [CrossRef]
62. Kutzbach, L.; Schneider, J.; Sachs, T.; Giebels, M.; Nykänen, H.; Shurpali, N.J.; Martikainen, P.J.; Alm, J.; Wilmking, M. CO_2 Flux Determination by Closed-Chamber Methods Can Be Seriously Biased by Inappropriate Application of Linear Regression. *Biogeosciences* **2007**, *4*, 1005–1025. [CrossRef]
63. Chiodini, G.; Cioni, R.; Guidi, M.; Raco, B.; Marini, L. Soil CO2 Flux Measurements in Volcanic and Geothermal Areas. *Appl. Geochem.* **1998**, *13*, 543–552. [CrossRef]
64. Bagnato, E.; Barra, M.; Cardellini, C.; Chiodini, G.; Parello, F.; Sprovieri, M. First Combined Flux Chamber Survey of Mercury and CO2 Emissions from Soil Diffuse Degassing at Solfatara of Pozzuoli Crater, Campi Flegrei (Italy): Mapping and Quantification of Gas Release. *J. Volcanol. Geotherm. Res.* **2014**, *289*, 26–40. [CrossRef]
65. Heinemeyer, A.; McNamara, N.P. Comparing the Closed Static versus the Closed Dynamic Chamber Flux Methodology: Implications for Soil Respiration Studies. *Plant Soil* **2011**, *346*, 145–151. [CrossRef]
66. Kyllönen, K.; Hakola, H.; Hellén, H.; Korhonen, M.; Verta, M. Atmospheric Mercury Fluxes in a Southern Boreal Forest and Wetland. *Water. Air Soil Pollut.* **2012**, *223*, 1171–1182. [CrossRef]
67. Liu, Y.; Wang, C.; Ding, L.; Wang, Z.; Teng, G.; Shi, Z.; Li, B. Influence of Deployment Time and Surface Wind Speed on the Accuracy of Measurements of Greenhouse Gas Fluxes Using a Closed Chamber Method under Low Surface Wind Speed. *J. Air Waste Manag. Assoc.* **2019**, *69*, 209–219. [CrossRef] [PubMed]
68. Sigler, J.M.; Lee, X. Gaseous Mercury in Background Forest Soil in the Northeastern United States. *J. Geophys. Res. Biogeosci.* **2006**, *111*, G02007. [CrossRef]
69. Zhou, J.; Wang, Z.; Zhang, X.; Driscoll, C.T. Measurement of the Vertical Distribution of Gaseous Elemental Mercury Concentration in Soil Pore Air of Subtropical and Temperate Forests. *Environ. Sci. Technol.* **2021**, *55*, 2132–2142. [CrossRef]
70. Heiri, O.; Lotter, A.F.; Lemcke, G. Loss on Ignition as a Method for Estimating Organic and Carbonate Content in Sediments: Reproducibility and Comparability of Results. *J. Paleolimnol.* **2001**, *25*, 101–110. [CrossRef]
71. Edmeades, D.C.; Wheeler, D.M. Measurement of Ph in New Zealand Soils: An Examination of the Effect of Electrolyte, Electrolyte Strength, and Soil:Solution Ratio. *N. Zeal. J. Agric. Res.* **1990**, *33*, 105–109. [CrossRef]
72. Mashyanov, N.R.; Pogarev, S.E.; Panova, E.G.; Panichev, N.; Ryzhov, V. Determination of Mercury Thermospecies in Coal. *Fuel* **2017**, *203*, 973–980. [CrossRef]
73. Petranich, E.; Predonzani, S.; Acquavita, A.; Mashyanov, N.; Covelli, S. Rapid Thermoscanning Technique for Direct Analysis of Mercury Species in Contaminated Sediments: From Pure Compounds to Real Sample Application. *Appl. Geochem.* **2022**, *143*, 105393. [CrossRef]
74. Biester, H.; Scholz, C. Determination of Mercury Binding Forms in Contaminated Soils: Mercury Pyrolysis versus Sequential Extractions. *Environ. Sci. Technol.* **1997**, *31*, 233–239. [CrossRef]
75. USDA Textural Soil Classification Study Guide. *Soil Mechanics Level I Module 3*; USDA Soil Conservation Service: Washington, DC, USA, 1987; pp. 1–53.
76. Ballabio, C.; Jiskra, M.; Osterwalder, S.; Borrelli, P.; Montanarella, L.; Panagos, P. A Spatial Assessment of Mercury Content in the European Union Topsoil. *Sci. Total Environ.* **2021**, *769*, 144755. [CrossRef] [PubMed]
77. Biester, H.U.; Muller, G.; Scholer, H.F. Binding and Mobility of Mercury in Soils Contaminated by Emissions from Chlor-Alkali Plants. *Sci. Total Environ.* **2002**, *284*, 191–203. [CrossRef] [PubMed]
78. Coufalík, P.; Komárek, J. The Use of Thermal Desorption in the Speciation Analysis of Mercury in Soil, Sediments and Tailings. *J. Anal. Chem.* **2014**, *69*, 1123–1129. [CrossRef]
79. Reis, A.T.; Coelho, J.P.; Rucandio, I.; Davidson, C.M.; Duarte, A.C.; Pereira, E. Thermo-Desorption: A Valid Tool for Mercury Speciation in Soils and Sediments? *Geoderma* **2015**, *237*, 98–104. [CrossRef]

80. Rumayor, M.; Lopez-Anton, M.A.; Díaz-Somoano, M.; Maroto-Valer, M.M.; Richard, J.H.; Biester, H.; Martínez-Tarazona, M.R. A Comparison of Devices Using Thermal Desorption for Mercury Speciation in Solids. *Talanta* **2016**, *150*, 272–277. [CrossRef]
81. Yin, R.; Feng, X.; Wang, J.; Li, P.; Liu, J.; Zhang, Y.; Chen, J.; Zheng, L.; Hu, T. Mercury Speciation and Mercury Isotope Fractionation during Ore Roasting Process and Their Implication to Source Identification of Downstream Sediment in the Wanshan Mercury Mining Area, SW China. *Chem. Geol.* **2013**, *336*, 72–79. [CrossRef]
82. Enescu, M.; Nagy, K.L.; Manceau, A. Nucleation of Mercury Sulfide by Dealkylation. *Sci. Rep.* **2016**, *6*, 39359. [CrossRef]
83. Biester, H.; Gosar, M.; Müller, G. Mercury Speciation in Tailings of the Idrija Mercury Mine. *J. Geochem. Explor.* **1999**, *65*, 195–204. [CrossRef]
84. Esbrí, J.M.; Bernaus, A.; Ávila, M.; Kocman, D.; García-Noguero, E.M.; Guerrero, B.; Gaona, X.; Álvarez, R.; Perez-Gonzalez, G.; Valiente, M.; et al. XANES Speciation of Mercury in Three Mining Districts—Almadén, Asturias (Spain), Idria (Slovenia). *J. Synchrotron Radiat.* **2010**, *17*, 179–186. [CrossRef]
85. Wallschläger, D.; Kock, H.H.; Schroeder, W.H.; Lindberg, S.E.; Ebinghaus, R.; Wilken, R.D. Estimating Gaseous Mercury Emissions from Contaminated Floodplain Soils to the Atmosphere with Simple Field Measurement Techniques. *Water. Air Soil Pollut.* **2002**, *135*, 39–54. [CrossRef]
86. Rinklebe, J.; During, A.; Overesch, M.; Wennrich, R.; Stärk, H.J.; Mothes, S.; Neue, H.U. Optimization of a Simple Field Method to Determine Mercury Volatilization from Soils-Examples of 13 Sites in Floodplain Ecosystems at the Elbe River (Germany). *Ecol. Eng.* **2009**, *35*, 319–328. [CrossRef]
87. Eckley, C.S.; Tate, M.T.; Lin, C.J.; Gustin, M.; Dent, S.; Eagles-Smith, C.; Lutz, M.A.; Wickland, K.P.; Wang, B.; Gray, J.E.; et al. Surface-Air Mercury Fluxes across Western North America: A Synthesis of Spatial Trends and Controlling Variables. *Sci. Total Environ.* **2016**, *568*, 651–665. [CrossRef]
88. Edwards, G.C.; Howard, D.A. Air-Surface Exchange Measurements of Gaseous Elemental Mercury over Naturally Enriched and Background Terrestrial Landscapes in Australia. *Atmos. Chem. Phys.* **2013**, *13*, 5325–5336. [CrossRef]
89. Lin, C.J.; Gustin, M.S.; Singhasuk, P.; Eckley, C.; Miller, M. Empirical Models for Estimating Mercury Flux from Soils. *Environ. Sci. Technol.* **2010**, *44*, 8522–8528. [CrossRef]
90. Fernández-Martínez, R.; Esbrí, J.M.; Higueras, P.; Rucandio, I. Comparison of Mercury Distribution and Mobility in Soils Affected by Anthropogenic Pollution around Chloralkali Plants and Ancient Mining Sites. *Sci. Total Environ.* **2019**, *671*, 1066–1076. [CrossRef]
91. O'Connor, D.; Hou, D.; Ok, Y.S.; Mulder, J.; Duan, L.; Wu, Q.; Wang, S.; Tack, F.M.G.; Rinklebe, J. Mercury Speciation, Transformation, and Transportation in Soils, Atmospheric Flux, and Implications for Risk Management: A Critical Review. *Environ. Int.* **2019**, *126*, 747–761. [CrossRef] [PubMed]
92. Schlüter, K. Review: Evaporation of Mercury from Soils. An Integration and Synthesis of Current Knowledge. *Environ. Geol.* **2000**, *39*, 249–271. [CrossRef]
93. Jiskra, M.; Wiederhold, J.G.; Skyllberg, U.; Kronberg, R.M.; Hajdas, I.; Kretzschmar, R. Mercury Deposition and Re-Emission Pathways in Boreal Forest Soils Investigated with Hg Isotope Signatures. *Environ. Sci. Technol.* **2015**, *49*, 7188–7196. [CrossRef]
94. Gabriel, M.C.; Williamson, D.G. Principal Biogeochemical Factors Affecting the Speciation and Transport of Mercury through the Terrestrial Environment. *Environ. Geochem. Health* **2004**, *26*, 421–434. [CrossRef]
95. Eckley, C.S.; Blanchard, P.; McLennan, D.; Mintz, R.; Sekela, M. Soil-Air Mercury Flux near a Large Industrial Emission Source before and after Closure (Flin Flon, Manitoba, Canada). *Environ. Sci. Technol.* **2015**, *49*, 9750–9757. [CrossRef]
96. Pannu, R.; Siciliano, S.D.; O'Driscoll, N.J. Quantifying the Effects of Soil Temperature, Moisture and Sterilization on Elemental Mercury Formation in Boreal Soils. *Environ. Pollut.* **2014**, *193*, 138–146. [CrossRef]
97. Carpi, A.; Lindberg, S.E. Application of a Teflon® Dynamic Flux Chamber for Quantifying Soil Mercury Flux: Tests and Results over Background Soil. *Atmos. Environ.* **1998**, *32*, 873–882. [CrossRef]
98. Gustin, M.S.; Biester, H.; Kim, C.S. Investigation of the Light-Enhanced Emission of Mercury from Naturally Enriched Substrates. *Atmos. Environ.* **2002**, *36*, 3241–3254. [CrossRef]
99. Llanos, W.; Kocman, D.; Higueras, P.; Horvat, M. Mercury Emission and Dispersion Models from Soils Contaminated by Cinnabar Mining and Metallurgy. *J. Environ. Monit.* **2011**, *13*, 3460–3468. [CrossRef]
100. Gómez-Armesto, A.; Martínez-Cortizas, A.; Ferro-Vázquez, C.; Méndez-López, M.; Arias-Estévez, M.; Nóvoa-Muñoz, J.C. Modelling Hg Mobility in Podzols: Role of Soil Components and Environmental Implications. *Environ. Pollut.* **2020**, *260*, 114040. [CrossRef]
101. Bavec, Š.; Gosar, M. Speciation, Mobility and Bioaccessibility of Hg in the Polluted Urban Soil of Idrija (Slovenia). *Geoderma* **2016**, *273*, 115–130. [CrossRef]
102. Ma, M.; Sun, T.; Du, H.; Wang, D. A Two-Year Study on Mercury Fluxes from the Soil under Different Vegetation Cover in a Subtropical Region, South China. *Atmosphere* **2018**, *9*, 30. [CrossRef]
103. Moore, C.; Carpi, A. Mechanisms of the Emission of Mercury from Soil: Role of UV Radiation. *J. Geophys. Res. Atmos.* **2005**, *110*, D24302. [CrossRef]
104. Choi, H.D.; Holsen, T.M. Gaseous Mercury Fluxes from the Forest Floor of the Adirondacks. *Environ. Pollut.* **2009**, *157*, 592–600. [CrossRef] [PubMed]
105. Fu, X.; Feng, X.; Wang, S. Exchange Fluxes of Hg between Surfaces and Atmosphere in the Eastern Flank of Mount Gongga, Sichuan Province, Southwestern China. *J. Geophys. Res. Atmos.* **2008**, *113*, D20306. [CrossRef]

106. Kuiken, T.; Zhang, H.; Gustin, M.; Lindberg, S. Mercury Emission from Terrestrial Background Surfaces in the Eastern USA. Part I: Air/Surface Exchange of Mercury within a Southeastern Deciduous Forest (Tennessee) over One Year. *Appl. Geochem.* **2008**, *23*, 345–355. [CrossRef]
107. Windmöller, C.C.; Durão, W.A.; de Oliveira, A.; do Valle, C.M. The Redox Processes in Hg-Contaminated Soils from Descoberto (Minas Gerais, Brazil): Implications for the Mercury Cycle. *Ecotoxicol. Environ. Saf.* **2015**, *112*, 201–211. [CrossRef]
108. Higueras, P.; Llanos, W.; García, M.E.; Millán, R.; Serrano, C. Mercury Vapor Emissions from the Ingenios in Potosí (Bolivia). *J. Geochem. Explor.* **2012**, *116–117*, 1–7. [CrossRef]
109. Jiang, T.; Skyllberg, U.; Wei, S.; Wang, D.; Lu, S.; Jiang, Z.; Flanagan, D.C. Modeling of the Structure-Specific Kinetics of Abiotic, Dark Reduction of Hg(II) Complexed by O/N and S Functional Groups in Humic Acids While Accounting for Time-Dependent Structural Rearrangement. *Geochim. Cosmochim. Acta* **2015**, *154*, 151–167. [CrossRef]
110. Fu, X.; Feng, X.; Zhang, H.; Yu, B.; Chen, L. Mercury Emissions from Natural Surfaces Highly Impacted by Human Activities in Guangzhou Province, South China. *Atmos. Environ.* **2012**, *54*, 185–193. [CrossRef]
111. Yuan, W.; Wang, X.; Lin, C.J.; Sommar, J.; Lu, Z.; Feng, X. Process Factors Driving Dynamic Exchange of Elemental Mercury Vapor over Soil in Broadleaf Forest Ecosystems. *Atmos. Environ.* **2019**, *219*, 117047. [CrossRef]
112. Gruba, P.; Socha, J.; Pietrzykowski, M.; Pasychnyk, D. Tree Species Affects the Concentration of Total Mercury (Hg) in Forest Soils: Evidence from a Forest Soil Inventory in Poland. *Sci. Total Environ.* **2019**, *647*, 141–148. [CrossRef] [PubMed]
113. Richardson, J.B.; Friedland, A.J. Mercury in Coniferous and Deciduous Upland Forests in Northern New England, USA: Implications of Climate Change. *Biogeosciences* **2015**, *12*, 6737–6749. [CrossRef]
114. Schuster, E. The Behavior of Mercury in the Soil with Special Emphasis on Complexation and Adsorption Processes—A Review of the Literature. *Water Air Soil Pollut.* **1991**, *56*, 667–680. [CrossRef]
115. Yang, Y.K.; Zhang, C.; Shi, X.; Lin, T.; Wang, D. yong Effect of Organic Matter and PH on Mercury Release from Soils. *J. Environ. Sci.* **2007**, *19*, 1349–1354. [CrossRef] [PubMed]
116. Barnett, M.O.; Harris, L.A.; Turner, R.R.; Stevenson, R.J.; Henson, T.J.; Melton, R.C.; Hoffman, D.P. Formation of Mercuric Sulfide in Soil. *Environ. Sci. Technol.* **1997**, *31*, 3037–3043. [CrossRef]
117. Carpi, A.; Fostier, A.H.; Orta, O.R.; dos Santos, J.C.; Gittings, M. Gaseous Mercury Emissions from Soil Following Forest Loss and Land Use Changes: Field Experiments in the United States and Brazil. *Atmos. Environ.* **2014**, *96*, 423–429. [CrossRef]
118. Mazur, M.; Mitchell, C.P.J.; Eckley, C.S.; Eggert, S.L.; Kolka, R.K.; Sebestyen, S.D.; Swain, E.B. Gaseous Mercury Fluxes from Forest Soils in Response to Forest Harvesting Intensity: A Field Manipulation Experiment. *Sci. Total Environ.* **2014**, *496*, 678–687. [CrossRef]